Chiral p-wave superconductivity in twisted bilayer graphene from dynamical mean field theory

B. Pahlevanzadeh[1,2], P. Sahebsara[1], D. Sénéchal[2*]

1 Department of physics, Isfahan University of Technology, Isfahan, Iran
2 Département de physique and Institut quantique, Université de Sherbrooke, Sherbrooke, Québec, Canada J1K 2R1
* david.senechal@usherbrooke.ca

March 16, 2021

Abstract

We apply cluster dynamical mean field theory with an exact-diagonalization impurity solver to a Hubbard model for magic-angle twisted bilayer graphene, built on the tight-binding model proposed by Kang and Vafek [1]. This model applies to the magic angle 1.30°. We find that triplet superconductivity with $p+ip$ symmetry is stabilized by CDMFT, contrary to other triplet or singlet order parameters. A minimum of the order parameter exists close to quarter-filling and three-quarter filling, as observed in experiments.

Contents

---

1 Introduction

Twisted bilayer graphene (TBG) consists of two layers of graphene deposited on top of each other with a slight rotation, or twist. At commensurate twist angles, the bilayer forms a moiré pattern with a period that depends closely on the twist angle. It has been predicted that for some "magic angles", the resulting band structure has a few relatively flat bands at low energy, separated from the rest, thus forming an effective strongly interacting electronic system [2–4]. The physical realization of this occurred in 2018 when Cao *et al.* observed Mott behavior in quarter-filled TBG (filling is understood here in terms of the four low-energy bands) at some

symbol	value (meV)
$t_{13}[0,0] = \omega t_{13}[1,-1] = \omega^* t_{13}[1,0]$	-0.011
$t_{14}[0,0] = t_{14}[1,0] = t_{14}[1,-1]$	$0.0177 + 0.291i$
$t_{14}[2,-1] = t_{14}[0,1] = t_{14}[0,-1]$	$-0.1141 - 0.3479i$

Table 1: Hopping amplitudes used in this work. They are the most important amplitudes computed in Ref. [1]. Here $\omega = e^{2\pi i/3}$ and the vector $[a,b]$ following the symbol represents the bond vectors in the $(\mathbf{E}_1, \mathbf{E}_2)$ basis shown on Fig. 1. Note that $t_{23} = t_{14}^*$ and $t_{24} = t_{13}^*$.

magic angles [5] and detected superconductivity just away from that filling [6]. Superconductivity was also found at larger twist angles by applying pressure [7]. These discoveries have renewed theoretical research on this system, with the goal of understanding the origin of superconductivity in TBG [8–17]. Some authors have found triplet superconductivity to be dominant [9, 12, 13], others predict singlet superconductivity, specifically of the $d + id$ type [8, 14, 16, 17]. The great variety of effective models and methods used complicates the comparison between these works.

The difficulty here is two-fold: (i) to construct a model Hamiltonian that can reasonably represent this very complex system and (ii) to predict correctly, within that model, whether superconductivity arises, and if so, with what characteristics: Singlet or triplet, order parameter symmetry, etc.

Since magic angle TBG is a strongly correlated system, the natural course of study is to set up an effective low-energy Hamiltonian in the Wannier basis, as opposed to the Bloch basis [1, 18–20]. Since the moiré pattern of TBG forms a triangular lattice, it was initially thought that the effective Hamiltonian would be defined on that lattice, and indeed it was shown that the electron density associated with the low-energy bands is peaked around its sites. However, it was then shown that no Wannier basis satisfying the minimal symmetry requirements could be constructed on a triangular lattice; on the contrary, the Wannier states have to be defined on the plaquettes of a triangular lattice, which form a graphene-like (hexagonal) lattice.

We adopt as a starting point the model proposed by Kang and Vafek [1], itself based on the microscopic analysis of Moon and Koshino [19]. We then simply add a Hubbard U, local to each of the four Wannier states per unit cell, and apply cluster dynamical mean field theory (CDMFT) to this interacting model in order to probe specific superconducting states. We find that a superconducting state indeed exists around quarter filling and three-quarter filling and that it is a triplet state with $p + ip$ symmetry. This is the main conclusion of this work.

2 Low-energy model

There have been a few proposals for an effective tight-binding Hamiltonian describing the low-energy bands of TBG [1, 18–20]. We adopt in this work the model described in Ref. [1] and inspired by Ref. [19]. It is based on four Wannier orbitals per unit cell, with maximal symmetry, on an effective honeycomb lattice.

Fig. 1 offers a schematic view of the orbitals w_1 and w_3. Orbitals $w_2 = w_1^*$ and $w_4 = w_3^*$ are not shown. Ref. [1] computes a large number of hopping integrals, of which we will only retain the largest, as listed in Table 1.

Remarkably, the most important hopping terms are between w_1 and w_4 (and between w_2 and w_3), i.e., between graphene sublattices. It therefore makes sense physically to picture the

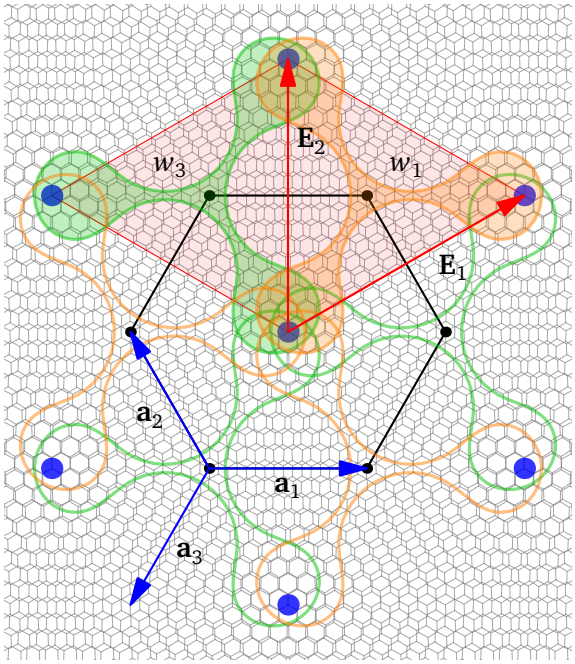

Figure 1: Schematic representation of the Wannier functions $w_1 = w_2^*$ (orange) and $w_3 = w_4^*$ (green) on which our model Hamiltonian is built. The charge is maximal at the AA superposition points (blue circles) forming a triangular lattice. The Wannier functions are centered on the triangular plaquettes that form a graphene-like lattice (black dots), whose unit cell is shaded in red. The underlying moiré pattern illustrated corresponds to $(m,n) = (9,8)$, but the functions used in this work correspond to $(m,n) = (26,25)$. The basis vectors $\mathbf{E}_{1,2}$ of the moiré lattice are shown (they are also basis vectors of the graphene-like lattice of Wannier functions), as well as the elementary nearest-neighbor vectors $\mathbf{a}_{1,2,3}$.

system as made of two *layers* and to assign w_1 and w_4 to the first layer, whereas w_2 and w_3 are assigned to the second layer. The concept of layer is useful when visualizing the model in space and when arranging local clusters of sites in CDMFT, since it is preferable to have the more important hopping terms within a cluster; it is merely a book-keeping device.

To this tight-binding model we will add a local interaction term U. We will defer the study of extended interactions (near-neighbor, etc.) to future work.

The model is invariant under a rotation C_3 by $2\pi/3$ about the AA site, and under a π-rotation C_2' about an axis in the plane of the bilayer (the vertical axis on Fig. 1). These transformations generate the point group D_3 and affect the Wannier orbitals as follows [1]:

$$\begin{aligned} C_3 &: w_1(\mathbf{r}) \to \omega w_1(C_3\mathbf{r}) & C_3 &: w_4(\mathbf{r}) \to \omega w_4(C_3\mathbf{r}) \\ C_3 &: w_2(\mathbf{r}) \to \bar{\omega} w_2(C_3\mathbf{r}) & C_3 &: w_3(\mathbf{r}) \to \bar{\omega} w_3(C_3\mathbf{r}) \\ C_2' &: w_1(\mathbf{r}) \to w_3(C_2'\mathbf{r}) & C_2' &: w_2(\mathbf{r}) \to w_4(C_2'\mathbf{r}) \end{aligned}$$

where $\omega = e^{2\pi i/3}$ and $\bar{\omega} = e^{-2\pi i/3}$. In other words, the orbitals w_1 and w_3 transform between themselves, and so do w_2 and w_4. The model also has time-reversal symmetry (TRS), under which $w_1 \leftrightarrow w_2$ and $w_3 \leftrightarrow w_4$.

Possible superconducting pairings are either singlet or triplet (there is no spin orbit coupling). It is reasonable to assume that pairing will be more important between sites that also correspond to the most important hopping integrals. Let us therefore concentrate on pairing states involving nearest neighbors on a given layer, i.e., between orbitals w_1 and w_4 (or w_2 and w_3). Because of the strong local repulsion in our model, we ignore on-site pairing. Let us then define the pairing operators

$$\begin{aligned} S_{i,\mathbf{r}} &= c_{\mathbf{r},\uparrow} c_{\mathbf{r}+\mathbf{a}_i,\downarrow} - c_{\mathbf{r},\downarrow} c_{\mathbf{r}+\mathbf{a}_i,\uparrow} \qquad \text{(singlet)} \\ T_{i,\mathbf{r}} &= c_{\mathbf{r},\uparrow} c_{\mathbf{r}+\mathbf{a}_i,\downarrow} + c_{\mathbf{r},\downarrow} c_{\mathbf{r}+\mathbf{a}_i,\uparrow} \qquad \text{(triplet)} \end{aligned} \tag{1}$$

where $c_{\mathbf{r},\sigma}$ annihilates an electron at graphene site $\mathbf{r}$ of the first layer (in orbital w_1 or w_4 depending on the sublattice). The elementary vectors $\mathbf{a}_i$ are defined on Fig. 1, but apply to the layer in the current context. Likewise, we define operators $S'_{i,\mathbf{r}}$ and $T'_{i,\mathbf{r}}$ on the second layer, in terms of orbitals w_2 and w_3). Under the transformations C_3 and C_2', the six singlet (triplet) pairing operators transform amongst themselves and may be organized into irreducible representations of D_3, as listed on Table 2. To make this table more concise, we have defined the following combinations:

$$s = \sum_{\mathbf{r}} \left(S_{1,\mathbf{r}} + S_{2,\mathbf{r}} + S_{3,\mathbf{r}} \right) \tag{2a}$$

$$d + id = \sum_{\mathbf{r}} \left(S_{1,\mathbf{r}} + \omega S_{2,\mathbf{r}} + \bar{\omega} S_{3,\mathbf{r}} \right) \tag{2b}$$

$$d - id = \sum_{\mathbf{r}} \left(S_{1,\mathbf{r}} + \bar{\omega} S_{2,\mathbf{r}} + \omega S_{3,\mathbf{r}} \right) \tag{2c}$$

$$f = \sum_{\mathbf{r}} \left(T_{1,\mathbf{r}} + T_{2,\mathbf{r}} + T_{3,\mathbf{r}} \right) \tag{2d}$$

$$p + ip = \sum_{\mathbf{r}} \left(T_{1,\mathbf{r}} + \omega T_{2,\mathbf{r}} + \bar{\omega} T_{3,\mathbf{r}} \right) \tag{2e}$$

$$p - ip = \sum_{\mathbf{r}} \left(T_{1,\mathbf{r}} + \bar{\omega} T_{2,\mathbf{r}} + \omega T_{3,\mathbf{r}} \right) \tag{2f}$$

and likewise for the combinations s', $d' \pm id'$, etc. for the second layer.

This organization into representations of D_3 is contingent on the importance of the inter-layer hopping t_{13}, which is an order of magnitude smaller than the intra-layer hopping. If

Irrep	singlet pairing	triplet pairing
A_1	$(d+id)+(d'-id')$	$(p+ip)-(p'-ip')$
A_2	$(d+id)-(d'-id')$	$(p+ip)+(p'-ip')$
E	$[d-id\ ,\ d'+id']$	$[p-ip\ ,\ p'+ip']$
	$[s,s']$	$[f,f']$

Table 2: Irreducible representations (irreps) of D_3 associated with the six pairing operators defined on nearest-neighbor sites, as defined in Eqs (2). (Un)primed operators belong to the second (first) layer.

t_{13} were zero, the two layers would be independent, the symmetry would be upgraded to C_{6v} and the classification of pairing states would be the same as in Ref. [21], with representations A_1 (s), A_2 (f), E_1 ($p \pm ip$) and E_2 ($d \pm id$). Since t_{13} is small, we expect that the different pairing states of Table 2 (for a given total spin) will be nearly impossible to differentiate from an energetics point of view, except for the difference between s and $d \pm id$ (or between f and $p \pm ip$).

3 Cluster dynamical mean field theory

In order to probe the possible existence of superconductivity in this model, we use cluster dynamical mean-field theory (CDMFT) [22–24] with an exact diagonalization solver at zero temperature (or ED-CDMFT). Let us summarize this method.

3.1 General description

The infinite lattice is tiled into identical, repeated units; this defines a superlattice, and an associated reduced Brillouin zone, smaller than the original Brillouin zone. In the present study the unit cell of the superlattice (or *supercell*) is made of four clusters of four sites each: Two clusters tile each of the two layers (Fig. 2c). Ref. [25] explains the particulars of CDMFT when the supercell contains more than one cluster. Each cluster is coupled to a bath of uncorrelated, auxiliary orbitals, and is governed by an Anderson impurity model (AIM):

$$H_{\text{imp}} = H_c + \sum_{i,r} \theta_{ir} \left(c_i^\dagger a_r + \text{H.c.} \right) + \sum_r \epsilon_r a_r^\dagger a_r, \tag{3}$$

where H_c is the infinite-lattice Hamiltonian, but restricted to the cluster, c_i annihilates an electron on orbital i of the cluster (i labels both site and spin) and a_r annihilates an electron on orbital r of the bath. The bath parameters (ϵ_r, θ_{ir}) are found by imposing a self-consistency condition, as explained below.

Hamiltonian (3) is solved by exact diagonalization. In particular, the electron Green function on the cluster, $\mathbf{G}_c(\omega)$, is computed. This is a $L_c \times L_c$ matrix, L_c being the number of orbitals on the cluster (including spin). It may be expressed in terms of the electron self-energy on cluster c, $\mathbf{\Sigma}_c(\omega)$, and the associated hybridization function $\mathbf{\Gamma}_c(\omega)$:

$$\mathbf{G}_c(\omega)^{-1} = \omega - \mathbf{t}_c - \mathbf{\Gamma}_c(\omega) - \mathbf{\Sigma}_c(\omega) \tag{4}$$

where

$$\Gamma_{c,ij}(\omega) = \sum_r \frac{\theta_{ir}\theta_{jr}^*}{\omega - \epsilon_r} \tag{5}$$

and $\mathbf{t}_c$ is the matrix of one-body terms of H_c (including the chemical potential μ).

The fundamental approximation of CDMFT is to replace the exact electron self-energy by the self-energy obtained by assembling the various cluster self-energies:

$$\mathbf{\Sigma}(\omega) = \bigoplus_c \mathbf{\Sigma}_c(\omega) \ , \tag{6}$$

where the direct sum is carried over the various clusters forming the supercell. The Green function on the infinite lattice is then approximated by

$$\mathbf{G}(\tilde{\mathbf{k}}, \omega) = \left[\omega - \mathbf{t}(\tilde{\mathbf{k}}) - \mathbf{\Sigma}(\omega)\right]^{-1} \ , \tag{7}$$

where $\tilde{\mathbf{k}}$ is a wavevector in the reduced Brillouin zone and $\mathbf{t}(\tilde{\mathbf{k}})$ is the noninteracting dispersion relation expressed in real space within the supercell and in reciprocal space within the reduced Brillouin zone. If $L_{\rm tot} = \sum_c L_c$ is the total number of orbitals in the supercell, then $\mathbf{G}(\tilde{\mathbf{k}}, \omega)$, $\mathbf{t}(\tilde{\mathbf{k}})$ and $\mathbf{\Sigma}(\omega)$ are $L_{\rm tot} \times L_{\rm tot}$ matrices. We further define the projected Green function

$$\bar{\mathbf{G}}(\omega) = \int \frac{d^2\tilde{k}}{(2\pi)^2} \mathbf{G}(\tilde{\mathbf{k}}, \omega) \tag{8}$$

This is the Fourier transform of the infinite-lattice Green function (7) to a single supercell around the origin. The CDMFT self-consistency condition requires that the $L_c \times L_c$ diagonal blocks of $\bar{\mathbf{G}}(\omega)$ (noted $\bar{\mathbf{G}}_c(\omega)$) should coincide with the corresponding cluster Green functions $\mathbf{G}_c(\omega)$. This cannot be satisfied exactly with a finite number of bath orbitals, because it should hold for all frequencies and only a finite number of bath parameters are at hand. Therefore this condition is replaced by the optimization of a distance function:

$$d(\boldsymbol{\epsilon}, \boldsymbol{\theta}) = \sum_{c, i\omega_n} W(i\omega_n) \left[\mathbf{G}_c(i\omega_n)^{-1} - \bar{\mathbf{G}}_c(i\omega_n)^{-1}\right] \tag{9}$$

where the weights $W(i\omega_n)$ are chosen in some appropriate way along a grid a Matsubara frequencies associated with some fictitious temperature β^{-1}. This is where some arbitrariness arises in the method, as will be commented below.

Let us then quickly summarize the actual CDMFT algorithm:

1. A trial value of the bath parameters (ϵ_r, θ_{ir}) is chosen. When looping over an external parameter, the previous converged value or an extrapolation thereof is chosen.

2. The cluster Green functions $\mathbf{G}_c(\omega)$ are computed, with the help of an *impurity solver* (here an exact diagonalization method).

3. The projected Green functions $\bar{\mathbf{G}}_c(\omega)$ are computed from Eqs (4), (7) and (8).

4. A new set of bath parameters is found by minimizing the distance function (9) with respect to the bath parameters entering $\mathbf{G}_c(\omega)$ through Eqs (4,5) for a fixed value of $\mathbf{\Sigma}_c$.

5. We go back to step 2 until the bath parameters or the hybridization functions $\mathbf{\Gamma}_c$ converge.

Once the converged solution is found, various quantities may be computed either from the impurity model ground state (averages, etc.) or from the associated lattice Green function $\mathbf{G}(\tilde{\mathbf{k}}, \omega)$.

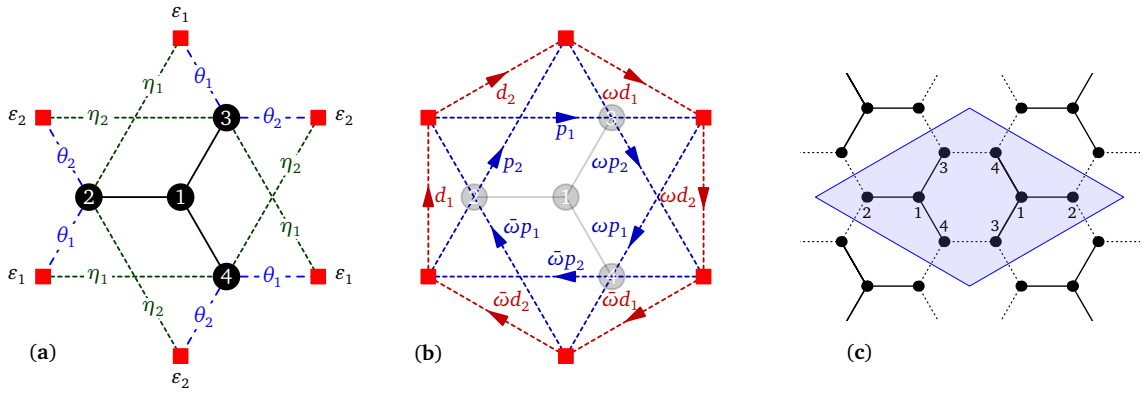

Figure 2: Schematic representation of the impurity model used in this work. Each cluster is made of four lattice sites (numbered black dots) and six bath orbitals (red squares). The normal-state bath parameters are shown on panel (a): Two different bath energies $\varepsilon_{1,2}$, four different hybridizations $\theta_{1,2}$ and $\eta_{1,2}$. The anomalous bath parameters are shown on panel (b). As shown, they are optimized for studying the $p+ip$ state: Two complex-valued triplet pairings $d_{1,2}$ between "nearest-neighbor" bath orbitals, and two other complex-valued triplet pairings $p_{1,2}$ between "second-neighbor" bath orbitals, all modulated by powers of the complex amplitude $\omega = e^{2\pi i/3}$ as one goes around ($\bar{\omega} = \omega^2 = \omega^{-1}$). The unit cell of the impurity model contains four copies of this cluster: Two on the bottom level ($w_{1,3}$), two on the top level ($w_{2,4}$). On each level, they are arranged as shown on panel (c) (the 4-site cluster on the right is the inversion of the one on the left, and the bath parameters are the same on the two clusters, except for the sign of the triplet pairings, which are inverted).

3.2 Cluster-bath system

The cluster-bath system for the current problem is illustated on Fig. 2. The supercell contains four 4-site clusters; one layer is illustrated on panel (c). Each cluster contains four sites and six bath orbitals and the various bath parameters are illustrated on panels (a) and (b). The four black, numbered circles are the cluster sites *per se*. The six red squares are the bath orbitals. Even though their positions have no meaning, they are, on this diagram, assigned a virtual position that makes them look as if they were physical sites on neighboring clusters. They are then given "nearest-neighbor" hybridizations $\theta_{1,2}$ and "second-neighbor" hybridizations $\eta_{1,2}$. In order to probe superconductivity, we add pairing amplitudes within the bath itself, as shown on Fig. 2b: Two pairing amplitudes $d_{1,2}$ between consecutive bath orbitals, and two others $p_{1,2}$ between "second neighbor" bath orbitals. In the context of Eq. (3), these pairing amplitudes must be understood in the restricted Nambu formalism, in which a particle-hole transformation is applied to the spin-down orbitals, giving the pairing operators the looks of hopping amplitudes. In total, the AIM contains 10 bath parameters, some real, some complex. The impurity Hamiltonian does not contain pairing operators on the cluster sites themselves. However, the operators defined in Eqs (1) may develop a nonzero expectation value on the impurity through the self-consistent bath.

The bybridization pattern shown in the figure is appropriate for triplet pairing (it is directional, as indicated by the arrows) in a $p+ip$ state (because of the phases ω and $\omega^2 = \bar{\omega}$ appearing in the bath pairing amplitudes as one circles around). This may be readily adapted to probing a $p-ip$ state (by replacing $\omega \leftrightarrow \bar{\omega}$) or a f state (by replacing $\omega, \bar{\omega} \to 1$). Likewise, singlet states are probed by introducing singlet pairing between bath sites. In principle, we could leave all pairings free, at the price of tripling the number of bath parameters, but CDMFT convergence has proven problematic when this was tested. It is easier, and no less general, to separately probe the $p \pm ip$ and f states (and likewise for the singlet states).

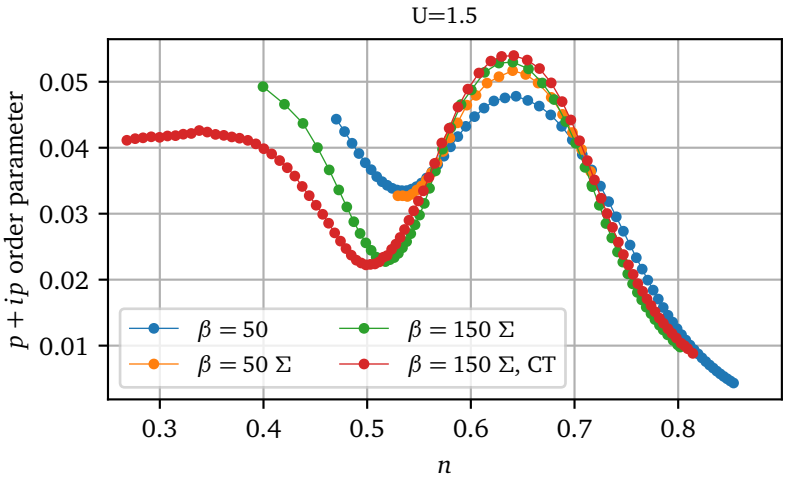

Figure 3: $p+ip$ order parameter found by CDMFT, as a function of electron density n, for $U = 1.5$ meV and several variants of the CDMFT procedure explained in the text. Only the hole-doped results ($n < 1$) are shown for clarity.

One could also treat the bath parameters of all four clusters of the supercell as independent. In practice, this is not necessary as they are related. The two clusters belonging to the same layer have identical bath parameters by symmetry, except for the triplet pairings which must change sign between the two clusters because the second cluster is obtained from the first by a spatial inversion. According to Table 2, we expect the complex-valued bath parameters of the second layer to be the complex conjugates of those of the first layer. These constraints effectively reduce the total number of variational parameters to the equivalent of 13 real parameters.

4 Results and discussion

We have probed the different states listed in Table 2 using the above CDMFT setup. In order to reach a solution from scratch, we have used the following staged approach: (i) Owing to the small value of t_{13}, a one-layer model was first studied. (ii) An external field of each of types (2) was then applied to the cluster in order to induce a nonzero average pairing forcefully. This external field was then reduced to zero in a few steps, each time starting from the previous solution. (iii) Once a nontrivial solution was found in this way at zero external field, the second-layer was added (with a complex conjugated bath system, e.g., $p-ip$ instead of $p+ip$). (iv) the solution found was then scanned as a function of chemical potential within the two-layer model.

We found a nonzero solution only for $p \pm ip$ pairing. Fig. 3 shows the average $p+ip$ order parameter on a cluster of the first layer, as a function of electron density on the cluster, for a local repulsion $U = 1.5$ meV. The order parameter is the ground-state expectation value of operator (2e) restricted to the cluster within the impurity model. Several variants of the CDMFT procedure are illustrated, which we must now explain. The distance function (9) depend on a set of weights $W(i\omega_n)$ and a fictitious temperature β^{-1}. The values of β (in meV^{-1}) are indicated in the legend of Fig. 3. The grid of Matsubara frequencies then stops at some cutoff value taken to be $\omega_c = 2$ meV in this work. The curve labelled $\beta = 50$ (blue dots) is obtained by setting all weights to the same value. The other curves (with a Σ label) are obtained by setting the weights proportional to the self-energy $|\mathbf{\Sigma}(i\omega_n)|$ (the norm of the matrix). This is justified

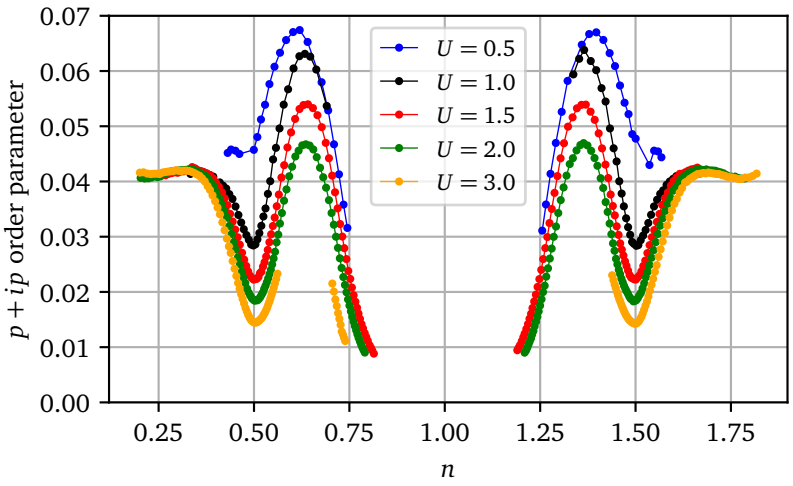

Figure 4: $p+ip$ order parameter found by CDMFT, as a function of electron density n, for several values of Hubbard U (in meV). The order parameter is the ground state average of the operator (2e), restricted to the cluster. The density n is the ground-state average occupation of the cluster. One of the clusters of the first layer was used for these averages. Clusters on the second layer would show the opposite chirality ($p-ip$).

if one considers DMFT from the point of view of the Potthoff functional [26,27]. In particular, it gives more importance to very low frequencies in an insulating state, as the self-energy then grows as $\omega \to 0$. We expect the superconducting order parameter to be minimum, if not zero, at quarter filling ($n = 0.5$), as observed in experiments. We see that this is not exactly the case in three of the four data sets of Fig. 3, although using a self-energy modulated set of weights and a higher β greatly helps. Upon studying the corresponding solutions, we observed that the electron density was not uniform on each cluster, the center site having a different density that the three sites at the edge. To offset this effect, we augmented the CDMFT procedure described in the previous section by imposing spatial uniformity. This was accomplished by adding to the impurity Hamiltonian (3) a counterterm:

$$H_{\mathrm{ct}} = \lambda[n_1 - \frac{1}{3}(n_2+n_3+n_4)] \tag{10}$$

where $n_a = \sum_{\sigma=\uparrow,\downarrow} c^\dagger_{a\sigma} c_{a\sigma}$ is the electron density at site a of the cluster, $a = 1$ being the center site. At each CDMFT iteration, the coupling λ is adjusted so as to steer the system towards $\langle H_{\mathrm{ct}}\rangle = 0$. The convergence on λ is carried at the same time as that of the bath parameters, so this procedure does not unduly increase computation time. Including this counterterm produces the red curve (labelled $\beta = 150$ Σ CT on Fig. 3), which shows a minimum of the order parameter exactly at quarter filling. This is the procedure that we followed to obtain the results shown on Fig. 4 for a few values of the on-site repulsion U.

Figure 4 shows the $p+ip$ order parameter as a function of electron density for the full range of solutions obtained, and five values of the one-site repulsion U (in meV). We note that the system is almost (but not exactly) particle-hole symmetric. Superconductivity is strongly suppressed near half-filling (CDMFT ceases to converge to a superconducting solution when $|n-1| \lesssim 0.2$). Superconductivity is partially suppressed at quarter- and three-quarter filling ($n = 0.5, 1.5$) and this suppression increases with U. Despite a strong suppression of superconductivity at $n = 0.5$ and $n = 1.5$, a Mott state is not fully obtained there for the range of U studied. This may be caused by our neglect of extended interactions.

We were not able to resolve the different representations of D_3, as listed on Table 2. In other words, the energy difference between the A_1, A_2 and E representations is too small to

have an effect on the CDMFT convergence procedure. This is due to the small value of the inter-layer hopping t_{13}. It is however important to assign opposite chiralities to the two layers. Note that convergence becomes more difficult at $U = 3$; the superconducting solution is not found in some doping range in that case. A weak singlet $(d + id)$ solution was also found in the vicinity of (but not at) half-filling when not imposing spatial uniformity. However, this solution disappeared once spatial uniformity was imposed by counterterms.

The effective model used was based on the parameters of Ref. [1], appropriate for a twist angle $\theta = 1.30°$. Would our conclusions change for different, small twist angles, such as the ones found in Ref. [6] ($\theta = 1.05°$, $1.16°$)? Maybe. But a similar CDMFT of the nearest-neighbor Hubbard model on the graphene lattice has shown triplet pairing to be dominant [21]; so did a RPA study of bi-layer silicene [28], which is likewise based on the graphene lattice. The effect of extended interactions remains to be studied; this is difficult in the CDMFT framework used here since important nearest-neighbor interactions (between the two layers) are not contained within the cluster, and therefore would require additional approximations that would confer a special status to the nearest-neighbor interactions located on the same cluster. This is deferred to future work.

Funding information DS acknowledges support by the Natural Sciences and Engineering Research Council of Canada (NSERC) under grant RGPIN-2015-05598. Computational resources were provided by Compute Canada and Calcul Québec

References

[1] J. Kang and O. Vafek, *Symmetry, Maximally Localized Wannier States, and a Low-Energy Model for Twisted Bilayer Graphene Narrow Bands*, Phys. Rev. X **8**(3), 031088 (2018), doi:10.1103/PhysRevX.8.031088.

[2] R. Bistritzer and A. H. MacDonald, *Moiré bands in twisted double-layer graphene*, PNAS **108**(30), 12233 (2011), doi:10.1073/pnas.1108174108.

[3] E. Suárez Morell, J. D. Correa, P. Vargas, M. Pacheco and Z. Barticevic, *Flat bands in slightly twisted bilayer graphene: Tight-binding calculations*, Phys. Rev. B **82**(12) (2010), doi:10.1103/PhysRevB.82.121407.

[4] G. Trambly de Laissardière, O. F. Namarvar, D. Mayou and L. Magaud, *Electronic properties of asymmetrically doped twisted graphene bilayers*, Phys. Rev. B **93**(23) (2016), doi:10.1103/PhysRevB.93.235135.

[5] Y. Cao, V. Fatemi, A. Demir, S. Fang, S. L. Tomarken, J. Y. Luo, J. D. Sanchez-Yamagishi, K. Watanabe, T. Taniguchi, E. Kaxiras, R. C. Ashoori and P. Jarillo-Herrero, *Correlated insulator behaviour at half-filling in magic-angle graphene superlattices*, Nature **556**, 80 (2018), doi:10.1038/nature26154.

[6] Y. Cao, V. Fatemi, S. Fang, K. Watanabe, T. Taniguchi, E. Kaxiras and P. Jarillo-Herrero, *Unconventional superconductivity in magic-angle graphene superlattices*, Nature **556**, 43 (2018), doi:10.1038/nature26160.

[7] M. Yankowitz, S. Chen, H. Polshyn, Y. Zhang, K. Watanabe, T. Taniguchi, D. Graf, A. F. Young and C. R. Dean, *Tuning superconductivity in twisted bilayer graphene*, Science **363**(6431), 1059 (2019), doi:10.1126/science.aav1910.

[8] D. M. Kennes, J. Lischner and C. Karrasch, *Strong correlations and $d + id$ superconductivity in twisted bilayer graphene*, Phys. Rev. B **98**(24), 241407 (2018), doi:10.1103/PhysRevB.98.241407.

[9] J. González and T. Stauber, *Kohn-Luttinger Superconductivity in Twisted Bilayer Graphene*, Phys. Rev. Lett. **122**(2), 026801 (2019), doi:10.1103/PhysRevLett.122.026801.

[10] B. Lian, Z. Wang and B. A. Bernevig, *Twisted Bilayer Graphene: A Phonon-Driven Superconductor*, Phys. Rev. Lett. **122**(25), 257002 (2019), doi:10.1103/PhysRevLett.122.257002.

[11] Z. A. H. Goodwin, F. Corsetti, A. A. Mostofi and J. Lischner, *Attractive electron-electron interactions from internal screening in magic-angle twisted bilayer graphene*, Phys. Rev. B **100**(23), 235424 (2019), doi:10.1103/PhysRevB.100.235424.

[12] B. Roy and V. Juričić, *Unconventional superconductivity in nearly flat bands in twisted bilayer graphene*, Phys. Rev. B **99**(12), 121407 (2019), doi:10.1103/PhysRevB.99.121407.

[13] Q.-K. Tang, L. Yang, D. Wang, F.-C. Zhang and Q.-H. Wang, *Spin-triplet f-wave pairing in twisted bilayer graphene near $\frac{1}{4}$-filling*, Phys. Rev. B **99**(9), 094521 (2019), doi:10.1103/PhysRevB.99.094521.

[14] L. Zhang, T. Huang, Y. Liang and T. Ma, *Ground state superconducting pair correlations in twisted bilayer graphene*, Mod. Phys. Lett. B **34**(01), 2050016 (2019), doi:10.1142/S0217984920500165.

[15] G. Sharma, M. Trushin, O. P. Sushkov, G. Vignale and S. Adam, *Superconductivity from collective excitations in magic-angle twisted bilayer graphene*, Phys. Rev. Research **2**(2), 022040 (2020), doi:10.1103/PhysRevResearch.2.022040.

[16] D. V. Chichinadze, L. Classen and A. V. Chubukov, *Nematic superconductivity in twisted bilayer graphene*, Phys. Rev. B **101**(22), 224513 (2020), doi:10.1103/PhysRevB.101.224513.

[17] W. Chen, Y. Chu, T. Huang and T. Ma, *Metal-insulator transition and dominant $d + id$ pairing symmetry in twisted bilayer graphene*, Phys. Rev. B **101**(15), 155413 (2020), doi:10.1103/PhysRevB.101.155413.

[18] M. Angeli, D. Mandelli, A. Valli, A. Amaricci, M. Capone, E. Tosatti and M. Fabrizio, *Emergent D_6 symmetry in fully relaxed magic-angle twisted bilayer graphene*, Phys. Rev. B **98**(23), 235137 (2018), doi:10.1103/PhysRevB.98.235137.

[19] P. Moon and M. Koshino, *Energy spectrum and quantum Hall effect in twisted bilayer graphene*, Phys. Rev. B **85**(19), 195458 (2012), doi:10.1103/PhysRevB.85.195458.

[20] N. F. Q. Yuan and L. Fu, *Model for the metal-insulator transition in graphene superlattices and beyond*, Phys. Rev. B **98**(4), 045103 (2018), doi:10.1103/PhysRevB.98.045103.

[21] J. P. L. Faye, P. Sahebsara and D. Sénéchal, *Chiral triplet superconductivity on the graphene lattice*, Phys. Rev. B **92**(8), 085121 (2015), doi:10.1103/PhysRevB.92.085121.

[22] G. Kotliar, S. Y. Savrasov, G. Pálsson and G. Biroli, *Cellular Dynamical Mean Field Approach to Strongly Correlated Systems*, Phys. Rev. Lett. **87**, 186401 (2001), doi:10.1103/PhysRevLett.87.186401.

[23] A. I. Lichtenstein and M. I. Katsnelson, *Antiferromagnetism and d-wave superconductivity in cuprates: A cluster dynamical mean-field theory*, Phys. Rev. B **62**(14), R9283 (2000), doi:10.1103/PhysRevB.62.R9283.

[24] D. Sénéchal, *Quantum cluster methods: CPT and CDMFT*, In E. Pavarini, E. Koch and P. Coleman, eds., *Many-Body Physics: From Kondo to Hubbard*, vol. 5, pp. 13.1–13.22. Forschungszentrum Jülich, ISBN 978-3-95806-074-6 (2015).

[25] M. Charlebois, D. Sénéchal, A.-M. Gagnon and A.-M. S. Tremblay, *Impurity-induced magnetic moments on the graphene-lattice Hubbard model: An inhomogeneous cluster dynamical mean-field theory study*, Phys. Rev. B **91**(3), 35132 (2015), doi:10.1103/PhysRevB.91.035132.

[26] M. Potthoff, M. Aichhorn and C. Dahnken, *Variational Cluster Approach to Correlated Electron Systems in Low Dimensions*, Phys. Rev. Lett. **91**(20), 206402 (2003), doi:10.1103/PhysRevLett.91.206402.

[27] D. Sénéchal, *Bath optimization in the cellular dynamical mean-field theory*, Phys. Rev. B **81**(23), 235125 (2010), doi:10.1103/PhysRevB.81.235125.

[28] L.-D. Zhang, F. Yang and Y. Yao, *Itinerant ferromagnetism and $p + ip$ superconductivity in doped bilayer silicene*, Phys. Rev. B p. 8 (2015), doi:10.1103/PhysRevB.92.104504.